

# Desiccation shrinkage of unconstrained soil in the saturated phase

L.B. Hu & T. Hueckel

*Duke University, Durham, North Carolina, USA*

H. Peron & L. Laloui

*EPFL, Lausanne, Switzerland*

**ABSTRACT:** Analysis of macroscopic desiccation shrinkage experiments indicates that most of the shrinkage occurs during drying while soil is still 100% wet. When air starts penetrating the soil, shrinkage practically ceases, while the water content is still above 20%. The remaining drying process occurs with a much-reduced shrinkage. In this context we look at the data of pore space evolution during saturated phase of drying as obtained via porosimetry. The observed behavior is modeled at a microscale using Poiseuille flow in capillary vessels with deformable walls driven by evaporation flux at the external boundary. A macroscopic model using Biot and Darcy theories for the continuum were recently presented by the authors.

## 1 INTRODUCTION

Desiccation phenomena in soils have been investigated for decades bringing progressively a better understanding of the mechanisms and physics involved (Abu-Hajleh & Znidarcic 1995, Kodikara et al. 1999, Konrad & Ayad 1997, Miller et al. 1998).

Recent desiccation experiments (Peron et al. 2006) on initially saturated soils near liquid limit point out to the conclusion that most of the shrinkage occurs during saturated phase of the process. This is in agreement with a general perception that unsaturated soil has a much higher stiffness than saturated soil. This is quite a universal behavior independently of the type of soil and type of pore fluid, as shown by Hu et al. 2007 (see Fig. 1). That includes shrinkage of soil permeated with ethanol solution, which has surface tension coefficient that is less than a half of that of water.

When soil becomes unsaturated, shrinkage practically stops, while the water content is still above 20%. The remaining drying process occurs with a much-reduced deformation. Hu et al. 2007 have also shown that the amount of deformation during the saturated drying and the shrinkage limit in terms of void ratio depend on the compressibility of the solid, but seems to be independent of surface tension and/or fluid saturation vapor pressure which characterizes evaporation process, or finally, from fluid viscosity. However, the rate of fluid loss and rate of shrinking are controlled by the evaporative and hydraulic conductivity properties, thus, those of the fluid. As it is generally agreed that capillary effects are caused by the fluid surface tension, it is postulated that the saturated phase of drying is largely independent from capillary effects, and shrinkage is due

to the fluid removal from the pore space via Darcian flow, while fluid-gas interface is confined to the external soil mass boundary, where all the phase transition takes place. Furthermore, possible capillary effects at the boundary appear to play a minor role in deformation, and hence the so-called “skin effect” is a negligible factor in deformation analysis.

A microscopic model of pore system deformation and transport is proposed to corroborate this hypothesis in relationship to the actual data on the evolution of the pore space.

A macroscopic counterpart model has been recently developed using Biot and Darcy theories by Hu et al. 2007.

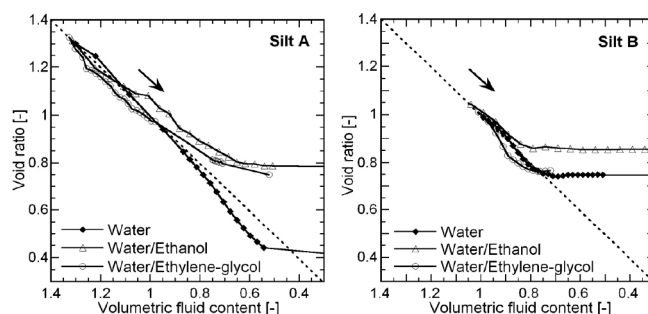


Figure. 1 Void ratio evolution during drying versus the volumetric fluid content change in clayey silt [Bioley silt] (left) and a granite powder (right) filled with water, water/ethanol 50-50 mixture and water-ethylene glycol 65-35 mixture (see Peron et al. 2007 for details)

### 2.1 Pore size distribution

Pore size distribution was obtained for Bioley clayey silt filled with water using Mercury Intrusion Porosimetry. The measurements were conducted at three stages of unconstrained desiccation: at the value of the water content of 33.1%, 24.8% and at 0.8%. These instants correspond to the initial state, near the shrinkage limit, and after the completion of the process. Fig. 2 visualizes the volume fraction for each instant. The evolution of the pore space can be summarized as follows: (1) the initial pore size is visibly bi-modal, with Large Pores (LP), ranging between  $0.6\mu\text{m}$  and  $3\mu\text{m}$  occupying initially 17% of the volumes of the medium, and Small Pores (SP), ranging between  $0.09\mu\text{m}$  and  $0.6\mu\text{m}$  occupying initially 21% of the volume of the medium. There are also minor volumes of peripheral size pores outside of the range of MIP, including those of clayey fraction (see Peron, 2008 for details). (2) At near shrinkage limit the LP take less than 5% of the volume of the medium, whereas the SP amount to 29%. Finally at near the completion of drying, the LP take less than 0.5% of the volume of the medium, whereas the SP still amount to 27%.

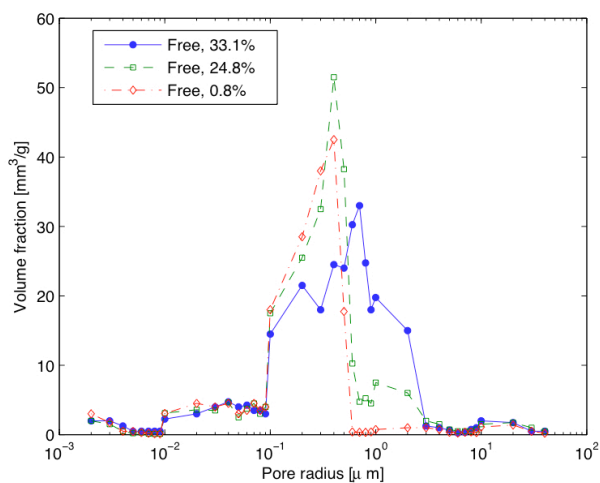


Figure 2. Pore size distribution evolution during drying of Bioley silt

### 2.2 Assessment of the pore space evolution during drying

This result is very significant, as it indicates that during the entire process the Small Pores do not decrease significantly, neither in size nor in total volume they occupy. To the contrary, at near shrinkage limit, they probably include the volume of former LP. The LP themselves practically all close during the saturated phase of drying and disappear at completion of the process. Similar results were recently

obtained by Cuisinier & Laloui (2004) and Koliiji et al. (2006) during suction induced desaturation process. Interestingly, it has been known for sometime that in bi-modal porosity soils, the SP remain virtually unchanged during consolidation process, whereas all volume changes are accommodated by LP (Delage & Lefebvre 1984). In reference to the desiccation process such evolution of the pore space implies that only the water volume contained in the LP is subject to evacuation during the saturated phase, and only that water volume produces the observed shrinkage.

## 3 MICROSCOPIC MODEL OF PORE SPACE EVOLUTION

### 3.1 Formulation

The above observations will be framed into a model of an evolving microscopic structure, based on the following specific postulates. It is recognized that the pore system of soil is made of sectors of straight tubes of two initial sizes: small (ST) and large (LT), with their internal diameters coinciding with the average values of the pore modes, identified in the preceding Section as  $0.5\mu\text{m}$  and  $1\mu\text{m}$ . The total initial volumes of the pores are set as equal to the initial value of the pore space of the corresponding modal volumes. The external radii of the tubes are not connected to any physical currently used characteristics of soils, except that the total volume of the solids of all the tubes must be representative of the total volume of the solids. Hence its value is determined as  $2.5\mu\text{m}$ . The grain size distribution data could provide some help, but not without a more extensive study.

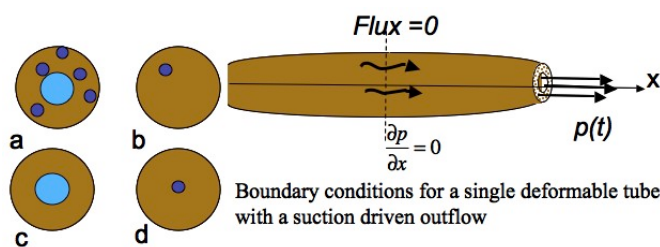


Figure 3. Schematics of a pore system in a cylindrical REV (a) and a BVP for a Small (b) eventually approximated via (d) and for a Large Pore (c).

To begin with we consider a representative elementary volume (REV) in a form of a single cylindrical deformable tube around a single cylindrical Large Pore located centrally and a series of parallel cylindrical Small Pores, all filled with water, and connected at their extremities to the atmosphere with which they can exchange gas and fluid. The tube representation is shown in Fig. 3a.

The solid of the tube represents a granular material, hence deforming irreversibly. The macroscopic experiments (see Peron et al. 2006) indicate that drying shrinkage strain is largely irreversible, while in the unsaturated phase the deformation is reversible to the state of the onset of desaturation, upon the removal of suction or re-wetting. The behavior of the solid material surrounding the pores will be considered as plastic, however it will be approximated via a linearly elastic law during loading and considered as perfectly rigid during an unloading. The adoption of a linear deformation law allows one to use a principle of superposition and hence represent the pore system of Fig. 3a as a superposition of effects of an LP and multiple SPs. Eventually for the reasons of simplicity SP will all be located centrally as well. Hence, the problem is reduced to that of a single tube with a single cylindrical pore.

The tube is considered as symmetric along and around its axis, loaded with a negative pore fluid pressure at the ends. It is assumed that a tube is completely filled with water during the considered phase (saturated). Water undergoes a viscous (Poiseuille) flow, i.e. an incompressible Newtonian fluid through a cylindrical tube. For the external boundary conditions for the fluid one can envision either a known (negative) water pressure history, or an imposed flux, resulting from the evaporation flux. The removal of water from the tube implies that its volume is compensated by the deformation of the tube. The time evolution of the negative pressure applied is reconstructed from the experiment (Peron et al. 2005, 2006) and shown in Fig. 4. At the axis of the symmetry at the tube half-length the no-flow condition is imposed.

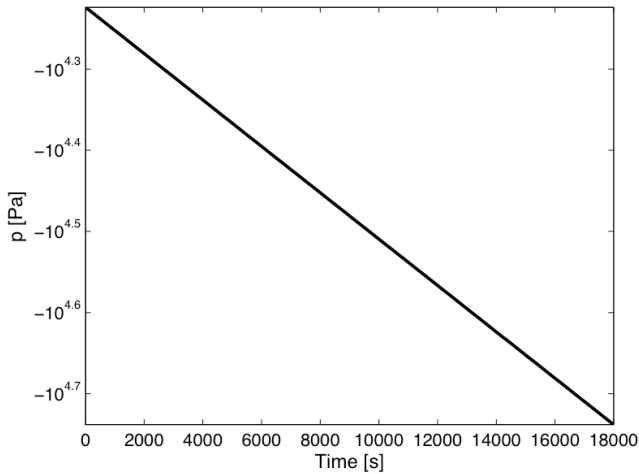


Figure 4. The negative pore pressure function imposed at the boundary  $x=L$  (from the experimental data)

Water transport in the tube is a viscous non-frictional (Poiseuille) flow with the externally applied negative pressure, which is evaporation-driven.

$$\frac{\partial p}{\partial x} = -\frac{8\mu}{\pi a^4} \dot{Q} = -\frac{8\mu}{a^2} F \quad (1)$$

$\dot{Q}$  is the volume-flow rate,  $F$  is the volume flux,  $p$  is water pressure,  $\mu$  is viscosity and  $a$  is the inner radius of the tube. We assume that the flow is solely attributed to the loss of volume of the inner conduit, i.e. due to the change in  $a$ , thus the volume change of an infinitesimal tube element per unit volume is

$$\frac{\partial v}{\partial t} = \frac{2\pi a}{\pi a^2} \frac{\partial a}{\partial t} = \frac{2}{a} \frac{\partial a}{\partial t} \quad (2)$$

And the mass conservation requires (in 1D)

$$\frac{\partial v}{\partial t} = -\frac{\partial F}{\partial x} \quad (3)$$

Thus substituting the flux into eq. (3), an approximate Poiseuille's equation for the collapsing tube is obtained

$$\frac{16\mu}{a^3} \frac{\partial a}{\partial t} = \frac{\partial^2 p}{\partial x^2} + \frac{2}{a} \frac{\partial a}{\partial x} \frac{\partial p}{\partial x} \quad (4)$$

It should be pointed out that a similar equation can also be obtained from eq. (1) by replacing the volume flow rate with the total volume loss of tube.

$$\dot{Q} = -\int_0^x 2\pi a \cdot \dot{a}(x,t) dx \quad (5)$$

In reality the tube radius  $a$  varies with  $x$  because of the elastic deformation in response to the variable (negative) pressure. A classical tube expansion/compression solution provides such a relationship. To further simplify the mathematical solution Fung (1984) expresses the change in radius as a function of the inner pressure by ignoring the radial strain

$$a(x) = a_0 \left[ 1 - \frac{a_0 p(x)}{Eh} \right]^{-1} \quad (6)$$

$E$  is the Young's modulus,  $a_0$  is the initial value of the inner radius  $a$ ,  $h$  is the thickness of the tube. Fung has shown that the latter approximation is very good, especially for low values of Poisson coefficient. As indicated in the subsequent context, the simulated deformation appears to be rather large, hence, a finite strain configuration may become a better approach. However, as our current priority in this paper is to examine the idea of using a deformable pore model to simulate the shrinkage, the mathematical merit of employing large deformation will be pursued in the future work.

Substituting (6) into the original eq. (4) produces a partial differential equation for pore pressure  $p$ .

$$\frac{\partial^2 p}{\partial x^2} + \frac{2a_0}{Eh \left[1 - \frac{pa_0}{Eh}\right]} \left(\frac{\partial p}{\partial x}\right)^2 = \frac{16\mu}{a} \frac{\left[1 - \frac{pa_0}{Eh}\right]}{Eh} \frac{\partial p}{\partial t} \quad (7)$$

The initial condition is: at  $t = 0, p = p_0 = 0$ . The boundary conditions are as follows:  $x = 0, \partial p / \partial x = 0$  and  $x = \pm L, p = p(t)$ , see Fig. 4.

Eq. (7) is a parabolic PDE. Its solution has been obtained using Matlab<sup>®</sup>.

### 3.2 Results

The solutions are obtained numerically for large and small pores separately. The numerical value of the deformability modulus  $E = 50$  KPa, and water viscosity chosen the same for the analyses of the LP and the SPs. The length of the tubes is 15 cm, taken as the length of the macroscopic experiments (see Peron et al. 2005). Both types of pores are subjected to the same external negative pressure evolution, as resulting from the same flux of water vapor (see Hu et al. 2007). The most significant difference between the two types of pores is in the amount of closure of the inner cavity: in 5 hours needed for reaching the shrinkage limit, the SP closes over  $0.08 \mu\text{m}$  from the original  $0.5 \mu\text{m}$  at the external boundary, whereas the LP closure amounts to  $0.33 \mu\text{m}$  from  $1 \mu\text{m}$ . This reflects correctly the porosimetry observation that the Large Pores convert into  $0.6 \mu\text{m}$  (or nearly Small Pore types) in that period of time.

The evolution of radii for selected cross sections of the tube proceeds similarly, but with a small but marked delay, as seen in Fig. 6a and b.

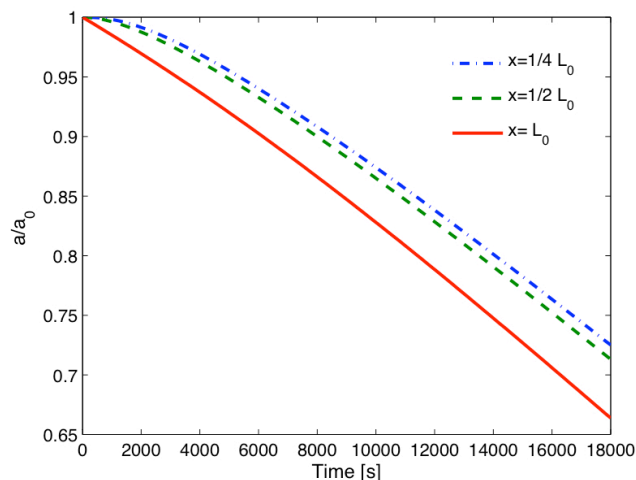


Figure.6a. Evolution of radii in LP at  $x=L, x=L/2$ , and  $x=L/4$

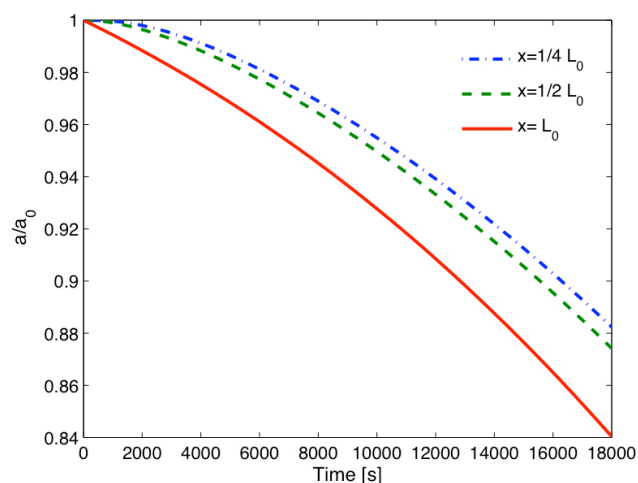


Figure.6b. Evolution of radii in SP at  $x=L, x=L/2$ , and  $x=L/4$

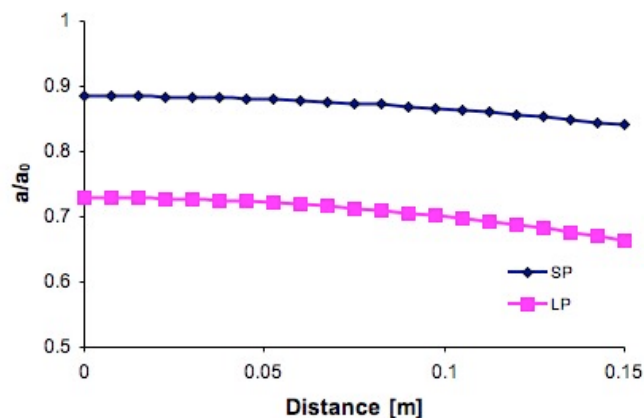


Figure 7. Radius profile for small and large pore after 5 hours of drying

The profiles of the opening along the axis for each pore type are shown in Fig. 7.

The results also indicate a different efficiency of SPs and LPs in transport of water toward the evaporating boundary. Fig. 8 shows water flux evolution at the boundary for both types of pore relative to their cross section surface area. A single LP provides more than twice of water than a SP after 5 hours.

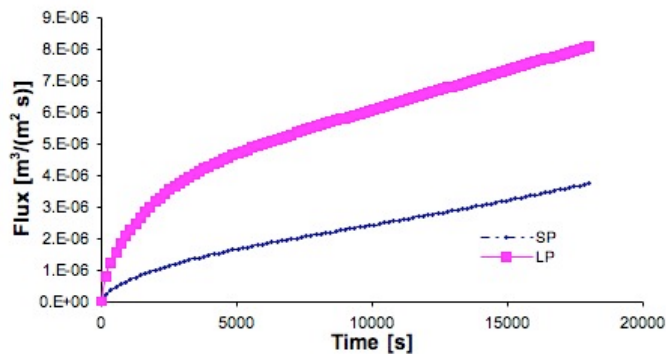


Figure 8. Water flux evolution at the external boundary for individual LP and SP

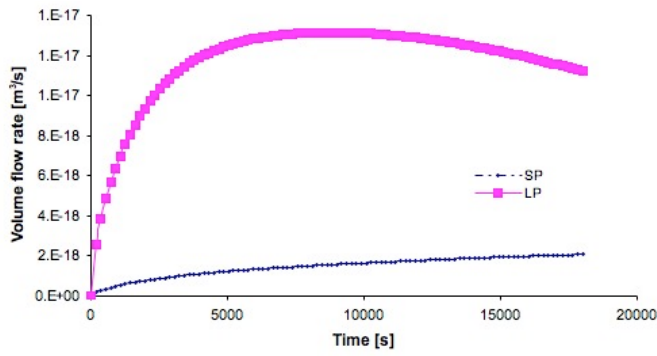


Figure 9. Volume flow rate evolution per single tube

Notably, as the areas of the individual tubes decrease in a significantly different manner, the volume flow rates per single tube yield a different picture (Fig. 9). Indeed, because of a large reduction of the cross section area of the large pore tube it appears that the latter reaches a maximum of the water output at about two hours from the onset of the process of drying. It may be expected that the small tubes reach a similar maximum at a later moment. Hence, the outflow from the system stabilizes and then gradually decreases, driven by the tube constriction. Whether this remains within the range of validity of the presented model remains an open question.

The cumulative volume loss via single LP and SP from the onset of evaporation is shown in Fig. 10.

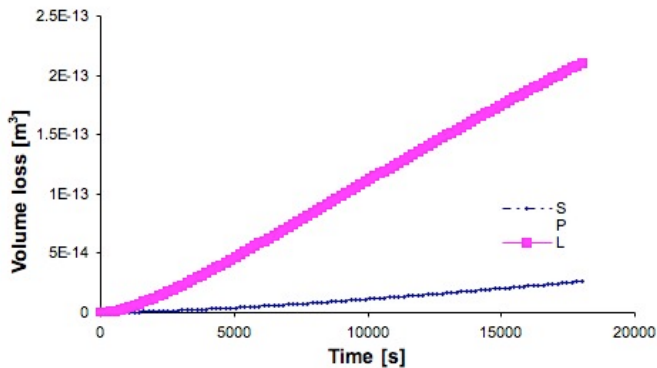


Figure 10. Cumulative volume output per single tube

On the mechanics side of the problem it is interesting to note that because of the common value of the externally applied negative pressure, both types of tubes are exposed to very similar pressure throughout almost the entire history of the drying process in the saturated range. Figures 11 and 12 present the evolution of such pressure along respectively LP and SP, indicating indeed very limited differences. It has to be realized however, that the two types of tubes have drastically different stiffness because of the differences in their thickness. This indeed produces such a dramatically different response in terms of the deformation of the tubes.

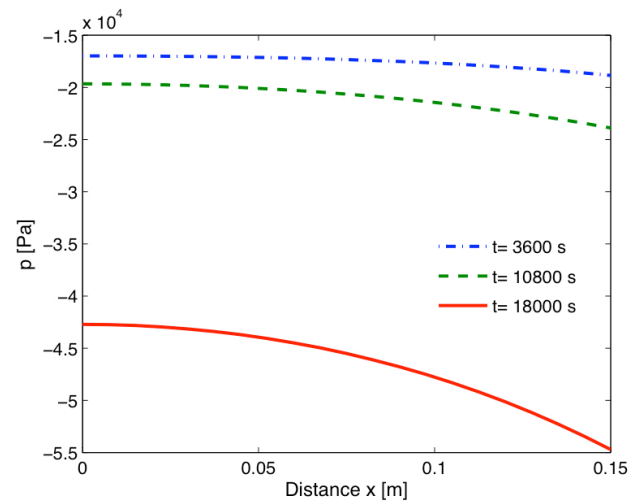


Figure 11. Small pore tube: evolution of the pressure profile along the tube axis

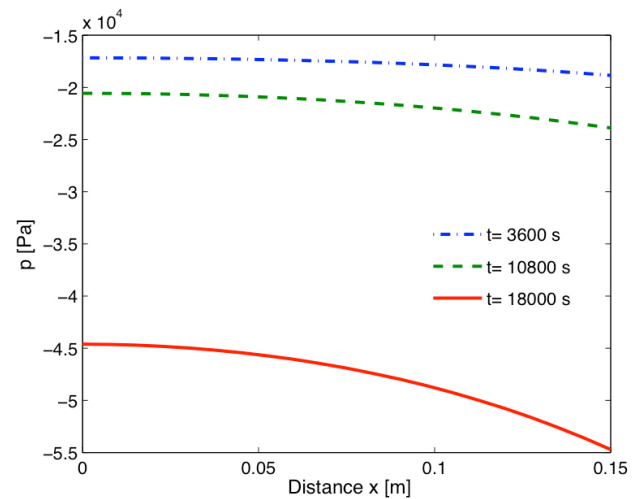


Figure 12. Large pore tube: evolution of the pressure profile along the tube axis

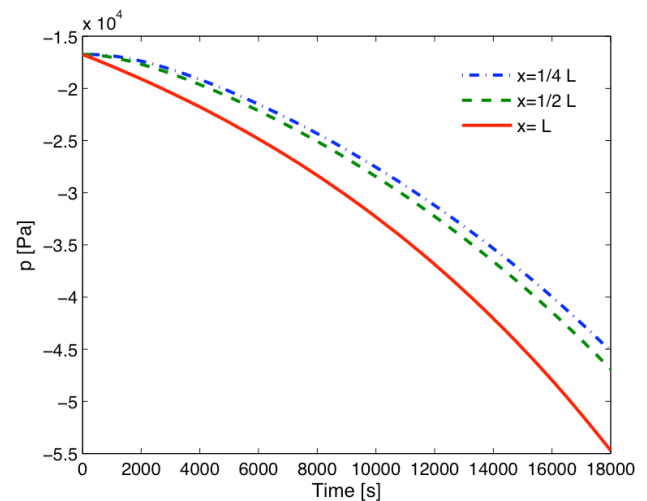


Figure 13. Evolution of pressure in LP at  $x = L/2$  and  $x = L/4$ . For comparison also the boundary pressure is shown

Finally, it is also seen that for selected cross sections of the tube the negative pressure evolves similarly, but with a marked delay, as visible in Fig. 13. In fact the pressure evolution mimics that of the radius of

the pore as may be expected from the form of eq. (6).

#### 4 DISCUSSION AND CONCLUSIONS

The presented microscopic model and numerical simulations of the drying process in its saturation phase indicate that the evolution of the highly idealized physical model reveals a series of characteristics that agree qualitatively with the experimental findings. The centerpiece of the model is transport of water toward the perimeter of the drying body producing the collapsing of the vessels. The model is largely based on the evolution of the pore system, idealized as bimodal. In particular, a significant reduction in diameter of large pores is seen, compared to that of smaller mode pores that is attributed to the difference in their deformability due to size difference.

Transport of water is characterized by an initial phase (two hours) when the discharge increases via large pores to stabilize at start to gently decrease after about four hours. An open question remains whether the aforementioned decrease remains within the range of the model validity.

Several simplifications and assumptions require further investigations, to start with the deformation modulus of the medium that comprises (only) smaller pores. An obvious limit of the validity of the model is the air entry moment. However, a microscopic criterion for this occurrence is still a point of discussion.

#### Acknowledgements

This work is funded by a cooperation between the Swiss National Science Foundation, grant 200020-109661 and the US National Science Foundation, grant # 0324543.

#### References

- Abu-Hajleh, A.N. & Znidarcic D. 1995, Desiccation theory for soft cohesive soils, *J. Geotech. Eng.* 121(6): 492 - 502
- Cuisinier, O. & Laloui, L. 2004, Fabric evolution during hydromechanical loading of a compacted silt, *Int. J. for Numerical and Analytical Methods in Geomechanics* 28: 483 – 499
- Delage, P. & Lefebvre, G., 1984, Study of the structure of the sensitive Champlain Clay and of its evolution during consolidation, *Canadian Geotechnical J.*, 21(1): 21 -35
- Fung, Y.C. 1984. *Biodynamics: Circulation*. New York: Springer
- Hu, L.B., Peron, H., Hueckel, T. & Laloui, L. 2006. Numerical and phenomenological study of desiccation of soil. In N. Lu, L.R. Hoyos and L. Reddi (eds.), *ASCE Geotechnical*

- Special Publication: Advances in Unsaturated Soil, Seepage, and Environmental Geotechnics*, 166-177
- Hu, L.B., Peron, H., Hueckel, T. & Laloui, L. 2007. Drying shrinkage of deformable porous media: mechanisms induced by the fluid removal. In H.W. Olson (ed.), *ASCE Geotechnical Special Publication 157: Geo-Denver 2007, New Peaks in Geotechnics*. 10 pages, CD-ROM
- Kodikara, J., Barbour, S.L. & Fredlund, D.G. 1999. “Changes in clay structure and behaviour due to wetting and drying.”. *Proceedings of the eighth Australia New Zealand Conference on Geomechanics*, Hobart, 1: 179-185.
- Koliji, A., Laloui, L. Cuisinier, O. & Vulliet, L. 2006, Suction Induced Effects on the Fabric of a Structured Soil, *Transport in Porous Media* 64: 261 -278
- Konrad, J.M. & Ayad, R. 1997. An idealized framework for the analysis of cohesive soils undergoing desiccation. *Canadian Geotechnical Journal* 34: 477-488
- Miller, C.J., Mi H. & Yesiller, N. 1998. Experimental analysis of desiccation crack propagation in clay liners. *Journal of the American Water Resources Association* 34(3): 677-686
- Peron, H. 2008. Ph.D. Thesis, Ecole Polytechnique Federal de Lausanne, ENAC, Lausanne, Switzerland, in preparation
- Peron, H., Laloui, L. & Hueckel, T. 2005. An experimental Evidence in Desiccation Cracking in Sandy Silt, in Tarantino, Romero and Cui (eds.), *Advanced Experimental Unsaturated Soil Mechanics*, Proceeding of Conference, Trento, Italy, April 2005, Taylor and Francis Group, London, 475 – 480
- Peron, H., Laloui, L., Hueckel, T. & Hu, L.B. 2006. Experimental study of desiccation of soil. In G.A. Miller, C.E. Zapata, S.L. Houston and D.G. Fredlund (eds.), *ASCE Geotechnical Special Publication 147: Unsaturated Soils 2006*, 1073-1084
- Peron, H., Hu, L.B., Hueckel, T. & Laloui, L. 2007. The influence of the pore fluid on desiccation of a deformable porous material. In T. Schanz (ed.), *Springer Proceedings in Physics, Experimental Unsaturated Soil Mechanics*, 413-420